L-cysteine modified acacia gum as a multifunctional binder for lithium-sulfur batteries

Qi Qi [a,‡], Yaqian Deng [a,‡], Sichen Gu [a,‡], Min Gao [d], Jun-ya Hasegawa [d], Guangmin Zhou [c], Xiaohui Lv [a], Wei Lv [a]* and Quan-Hong Yang [b]*

[a] Shenzhen Geim Graphene Center, Engineering Laboratory for Functionalized Carbon Materials, Tsinghua Shenzhen International Graduate School, Tsinghua University, Shenzhen 518055, Guangdong, China

[b] Nanoyang Group, State Key Laboratory of Chemical Engineering, School of Chemical Engineering and Technology, Tianjin University, Tianjin, 300072, China

[c] Tsinghua-Berkeley Shenzhen Institute (TBSI), Shenzhen International Graduate School, Tsinghua University, Shenzhen 518055, China

[d] Institute for Catalysis, Hokkaido University, Sapporo 001-0021, Japan

KEYWORDS: multifunctional binder, lithium-sulfur batteries, acacia gum, L-cysteine, modification

ABSTRACT: Binder plays important roles in stabilizing the electrode structure and improving the cyclic stability of batteries. However, the traditional binders are no longer satisfactory in lithium-sulfur (Li-S) batteries due to their failure in accommodating the large volume changes of sulfur

and trapping soluble intermediate polysulfides, thus causing severe capacity decay. In this work, we prepared a multifunctional binder for Li-S batteries by merely modifying the acacia gum, a low-cost biomass polymer, with L-cysteine under a mild condition. Owing to the introduced amino and carboxyl branches by the L-cysteine, the modified acacia gum shows enhanced polysulfides trapping ability and can effectively restrain the shuttling of polysulfides. In addition, the introduction of branches can help form a cross-linked 3D network with better mechanic strength and flexibility for adhering sulfur and accommodating the volume changes of cathode materials. As a result, compared with the normally used PVDF binder and the unmodified acacia gum binder, the L-cysteine modified acacia gum binder effectively enhanced the rate capability and cycling stability of the Li-S batteries directly using sulfur as the cathode, showing a promoting way to prompt the practical use of Li-S batteries.

INTRODUCTION

In these years, lithium-sulfur (Li-S) batteries attract great attention due to their high energy density and low cost compared with the widely used lithium-ion batteries, and show the potential of implication in large scale grid and portable electronic devices.[1-6] However, their practical applications are hindered by the fast capacity decay and sever side reactions resulting from the shuttling of soluble polysulfides (LiPSs) and the large volume change of cathode materials.[7-8] Incorporating hierarchical carbon frameworks[9] or chemical trappers[10] to sulfur is an effective strategy for accommodating volume change and suppressing the shuttling effects. However, manufacturing these hybrids always increases the cost and decreases the loading mass of active materials due to the large occupied weight/space of host materials, which can hardly meet the commercial requirements for practical batteries. In contrast, binder only accounts for a small

proportion in weight/mass in electrode, but plays a vital role in determining slurry properties, electrode structure and the ultimate electrochemical performance.[11-14] Thus, developing an advanced binder should be a more efficient strategy to improve the Li-S battery performance and promote its practical applications.

Polyvinylidene fluoride (PVDF) is the widely used binder in batteries, but it cannot well maintain the integrity of electrodes with large volume changes during cycling.[15] The water-soluble binders, such as sodium-alginate,[16] sodium carboxyl methyl cellulose (CMC),[17] and poly(ethylene oxide) (PVP)[18] have better flexibility to strengthen the electrode structure in Li-S batteries, but these binders are inferior in capturing LiPSs and hard to be functionalized due to the lack of active sites. In this case, the combination,[19] functionalization,[20] and structure modification[21] of binders were further studied to improve their performance, but these processes are usually too complicated to meet the requirements of future practical applications. Different from above binders, the Acacia gum (denoted AG), a non-toxic and water-soluble natural polymer extracted from Acacia Senegal, has a long D-galactopyranose backbone chain and side D-glucuronic acid, L-arabinofuranose and hydroxyproline groups,[22-23] which can adsorb the LiPSs and can be easily modified to introduce the functional groups. However, according to the previous report,[23-24] the LiPSs adsorption ability of AG should be mainly contributed by the -COOH groups which only account a small amount in the AG molecule, which leads to the inferior trapping ability towards LiPSs.

Herein, we developed an easy, low-cost method to modify AG, which endows its exceptional LiPSs capturing ability while maintaining its good binder functions. L-cysteine (denoted L-Cys) was used to realize the AG functionalization due to its good solubility in aqueous solution, simple molecular structure and rich functional groups (carboxyl, amino and sulfhydryl groups) having good LiPSs trapping ability, endowing the modified AG binder good solubility, enhanced binding

ability and the largely improved adsorption ability towards LiPSs. Amino groups were introduced in the side chains of AG under a mild condition (the obtained product was denoted as L-AG), which increased LiPSs adsorption ability and effectively suppressed their shuttling. Moreover, L-AG binder helped form 3D cross-linked binder network in the electrode due to the introduced side chains which endowed the electrode with better integrity and flexibility than PVDF and AG binders, and thus, the greatly enhanced rate performance and cycling stability of Li-S battery directly using sulfur as the cathode material were achieved.

EXPERIMENTAL SECTION

Preparation of L-AG and the cathode. In a typical process, AG (Aladdin) and L-Cys (Macklin) were dissolved in deionized water and magnetically stirred for 2 h at 70 °C, after which the solvent was evaporated to obtain 10 mL solution and form a solid precipitate. The supernatant was collected by filtration and was added to ethanol to achieve the precipitates of the binder of L-AG. The sulfur cathode was prepared by casting the slurry of mixed sulfur powder (56 wt%) as the active material, BP2000 (24 wt%) and graphene (10 wt%) as the conductive additives, and 10 wt% binders in N-methyl-2-pyrrolidone (for PVDF) or water (for AG and L-AG binders) onto the carbon-coated aluminum foil. The electrode was dried at 60 °C under vacuum for 12 h. After drying, the sulfur loadings in the electrodes with PVDF, AG and L-AG were about 55.24, 56.63 and 56.73 wt% according to the thermogravimetry (TG) results in Figure S1. The normal sulfur loading is ~1 mg cm^{-2} and the high sulfur loading is ~3 mg cm^{-2}.

Adsorption ability of LiPSs. Before the adsorption test, the binders were dried at 60 °C under vacuum overnight and 20 mg of each binder was added to the Li_2S_6 solution, which was prepared by mixing stoichiometric amount of Li_2S and sulfur in DOL/DME solution (1:1 v/v). The solution

was stirred overnight at 70 °C in glovebox to produce a 0.5 M Li_2S_6 solution and was then diluted to 1 mM for the test of polysulfide adsorption.

Adherence force test. A cross-cutting knife was used to draw 9 parallel lines on the electrode with different binders, and then draw 9 lines perpendicular to them forming an 8 × 8 grid (area size 1 mm × 1 mm). The 3 M tape was applied to the surface of the electrodes tightly and was quickly peeled off from the electrodes at a certain angle (60 °). The adherence of binders was evaluated by the peeling situation of electrodes based on the sulfur mass loadings.

Electrolyte uptake test. Electrodes using different binders were soaked in the electrolyte for 1 h, the changes of the electrode weight were measured after dried in air to remove the physically adsorbed electrolyte.

Computational details. All the calculations were performed by the density functional theory (DFT) method at B3LYP/6-311++G** level which is implemented in Gaussian 09 program package.[25] The charge distribution analysis was done by using natural bond orbital analysis.[26-27]

Materials characterization. The morphology and microstructure of the samples were characterized by Hitachi SU8010. Samples were directly adhered to the conductive paste. Fourier transform infrared spectrometry (FTIR) analyses were performed using a Nicolet IS50 infrared analyzer. UV-Vis absorption spectra were obtained with an Agilent Cary 5000 UV-visible-NIR spectrometer. TG was used to study the thermal stability of samples and sulfur loadings of the electrodes. The equipment used in this paper is the STA-499 F3 Jupiter® Synchronous Thermal Analyzer from NETZSCH, Germany, using Al_2O_3 crucible at a heating rate of 5 °C min^{-1} and a nitrogen atmosphere. X-ray photoelectron spectroscopy (XPS) analyses were carried out on a PHI 5000 VersaProbe II spectrometer using monochromatic Al Kα X-ray source.

Composition analysis. 300 mg samples were dissolved in 3 mL 72% H_2SO_4 and stirred 10 min at room temperature, and then heated to 121 °C for 1 h in a sterilizer. The obtained liquid was diluted 50 times with deionized water and 1 mL of it was passed through a 0.22 μm microfiltration membrane in a chromatographic analysis bottle. The above samples were quantified by a high-efficiency anion exchange chromatography system using a CarboPac PA 20 analytical column pulsed amperometric detection. Neutral sugar and glucuronic acid were separated with 18 mM NaOH and 0.3 M NaOH at the rate of 0.5 mL min^{-1}. The run time was 45 minutes, after which the column was rinsed with 0.2 M NaOH for 10 minutes and eluted with 18 mM NaOH for 15 minutes.

Viscosity test. The solutions with a concentration of 10 wt% binders were prepared and their viscosities were measured using a Brookfield DV-II viscosity meter.

Electrochemical measurements. The cells were assembled using a 2032 coin cells in a high-purity Ar-filled glove box by stacking lithium metal anode, Celgard 2500 membrane and cathode. The electrolyte was 1 M Lithium bis(trifluoromethane sulfonyl)imide (LiTFSI) in a solvent of 1,3-dioxolane (DOL) and dimethoxyethane (DME) (1:1 in weight) with 1 wt% $LiNO_3$ as additive. 20 μL of the electrolyte was added to both sides of the separator. The electrolyte: sulfur (E:S) ratio is 17 μL mg_s^{-1} for the normal electrode and 7 μL mg_s^{-1} for the high sulfur loading electrode. The galvanostatic charge-discharge tests were conducted on a LAND instrument with the potential range of 1.7-2.8 V (vs Li/Li^+). The rate performance for battery tests varied from 0.1 C to 2 C rate (1 C=1675 mA g^{-1}), according to the mass of sulfur loading. Cyclic voltammetry (CV) study of the electrode was recorded by a Biologic VMP3 multi-channel electrochemical workstation in the voltage range of 1.7-2.8 V (vs Li/Li^+) at a scan rate of 0.05 mV s^{-1}. Electrochemical impedance spectra were tested with the scan frequency range from 10 to 100 kHz recorded by a Biologic VMP3 multi-channel electrochemical workstation. The electrode for the electrochemical stability

test of L-AG was prepared by directly dissolving the mixture of BP2000, graphene and L-AG (weight ratio of 24:10:10) in water and casting the slurry on carbon-coated aluminum foil. Then, the electrode was tested by CV at 0.1 mV s^{-1} in the voltage window of 1.7-2.8 V.

RESULTS AND DISCUSSION

The reaction of L-Cys and AG was conducted in solution under 70 °C, as shown in Figure S2. The composition and chemical structures of L-AG, AG and L-Cys were characterized by the Fourier transform infrared spectroscopy (FTIR spectroscopy) and thermogravimetric analysis (TG). The peaks located at 1258 and 1616 cm^{-1} in the FTIR profiles of AG and L-AG are derived from the O-C-H deformation of pyranose rings and the symmetric vibrations of O-C-O bonds, respectively (Figure S3).[23] The peak at 1531 cm^{-1} of L-AG is related to the bending vibration of N-H bond,[28] and the weight loss peak at 220 °C in TG profile of L-AG (Figure S4) is related to the loss of -NH_2,[29] proving the introduction of -NH_2 in L-AG. As shown in Figure S5, the peak of C 1s at 285.6 eV is derived from the C-S bond.[20] In Figure 1d and Figure S6, the appeared peak at 163.3 eV in the S 2p XPS profile of L-AG should be ascribed to the C-S-C bond formed by the reaction between the mercapto group (-SH) of L-Cys and the hydroxyl (-OH) group of AG,[30] which is different from the C-S-H bond (164.4 eV) in L-Cys or the C-S-S-C bond (164.7 eV) (Figure S7) in the intermediate product L-cystine (denoted L-C), indicating the covalent bonding between AG and L-Cys.

The reaction between AG and L-Cys was further verified by the component analysis shown in Figure S8. The AG and L-AG will be hydrolyzed by sulfuric acid, and form monosaccharide components which can be detected in anion exchange chromatography measurement.[31] The content of arabinose derived from L-AG is lower than that from AG, suggesting the binding

between L-Cys and arabinose. Based on the above analysis, we can speculate the AG is functionalized by L-Cys through the reaction between the -SH in L-Cys and the -OH of arabinose in AG. After taking off one molecule of water, the C-S-C bond (Figure 1a) is formed.

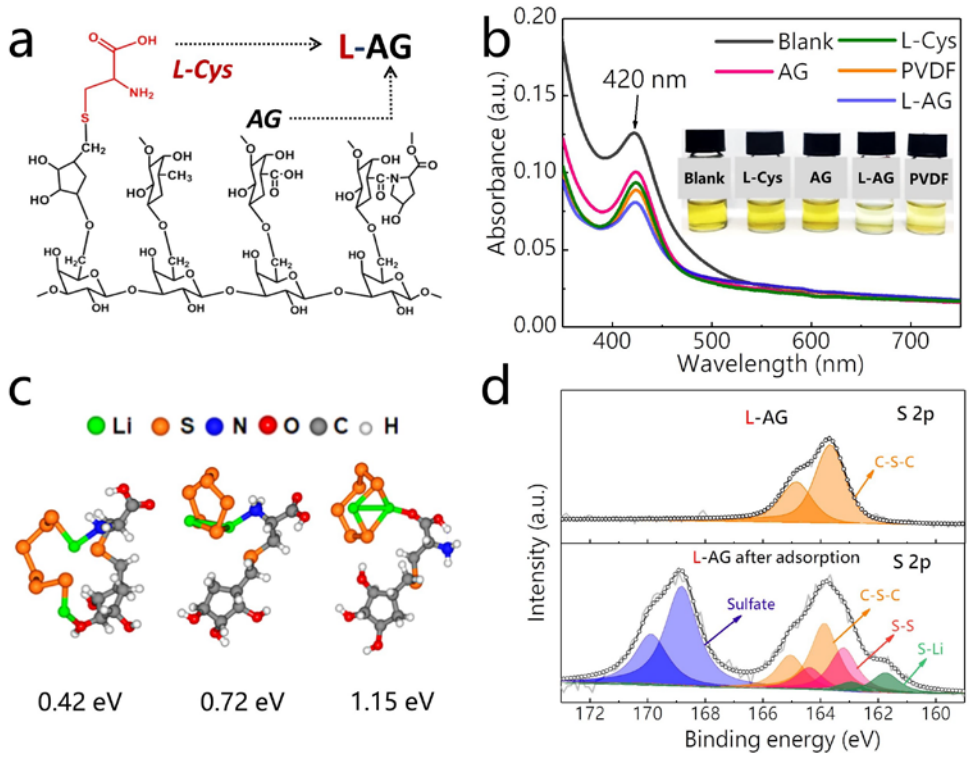

Figure 1. (a) The chemical structure of L-AG. (b) Photos of the Li_2S_6 (1 mM) adsorption by L-Cys, AG, L-AG and PVDF in DOL/DME solution and the UV-Vis curves of Li_2S_6 solution before and after adsorption. (c) Adsorption geometries and binding energies of Li_2S_6 on the $-NH_2$ and -COOH groups in L-AG. (d) The S 2p XPS profiles of L-AG and L-AG after Li_2S_6 adsorption.

The LiPSs adsorption ability of PVDF, L-Cys, AG and L-AG was evaluated by the static adsorption test in the DOL/DME (1:1) solution containing 1 mM Li_2S_6 (Figure 1b). It is shown that AG and L-Cys almost have no adsorption ability towards LiPSs. In contrast, L-AG shows much stronger adsorption ability of LiPSs than PVDF, L-Cys and AG, which should be attributed to the strong electrostatic attraction between Li^+ and negatively charged atom such as N^{3-} and O^{2-}

in introduced -NH_2 and -COOH.[32] Although L-Cys contains similar functional groups with L-AG, its small molecular structure makes it highly dispersible in the solvent as revealed by the UV-vis adsorption test in Figure 1b, resulting in weak trapping ability towards LiPSs in solution. For AG, though having a -COOH group on the chain, it shows poor adsorption ability, because the hydrophobic of hydroxyproline and the hydrophilic of polysaccharide chains make the AG molecules tightly aggregate and form intramolecular hydrogen bonds in the organic electrolyte, hindering the contact of functional groups with LiPSs.[33]

Density function theory (DFT) calculations were carried out to further investigate the adsorption effect of induced -COOH and -NH_2 groups on Li_2S_6. As shown in Figure S9a, various initial structures were considered to investigate the interaction between L-AG and Li_2S_6. The stable geometries and corresponding binding energies of L-AG-Li_2S_6 are illustrated in Figure 1c. It is shown that Li_2S_6 cluster prefers to bind to L-AG with a cyclic structure, which effectively suppresses the migration of LiPSs. In accordance with the experimental results, Li_2S_6 either binds to the O atoms of -COOH or the N atom of -NH_2 in L-AG with strong binding energies of 1.15 eV and 0.72 eV, respectively. This can be explained by the polarity of O and N atoms. As the natural Population Analysis in Figure S9a shows, both O and N atoms are negatively charged to attract the positive charged Li ions. The interaction between Li_2S_6 and AG was also investigated to reveal the interaction between Li_2S_6 and the -COOH group. Although the Li_2S_6 also binds with -COOH of AG, it presents much lower binding energy of 0.67 eV and longer bond length of Li-O (1.89 Å) than Li_2S_6-(L-AG) (1.15 eV, 1.85 Å), suggesting weaker electrostatic force between six-membered ring and Li_2S_6. Therefore, introducing L-Cys not only increases the adsorption sites but also increases the electrostatic force between L-AG and Li_2S_6. It can be expected that interaction between a binder and LiPSs can be effectively tuned by electron density substituted

groups. The adsorption abilities of introduced -COOH and -NH_2 groups with Li_2S_4 were also investigated. As shown in Figure S9b, the binding energies are 0.1 and 0.55 eV, respectively, which are smaller than those with Li_2S_6, showing they have much stronger adsorption ability with the highly soluble LiPSs.

XPS spectra were collected to further reveal the interaction between L-AG and LiPSs. As shown in Figure 1d, the peak at 163.3 eV, which is ascribed to C-S-C in L-AG, confirmed the functionalization reaction between -SH and -OH. After absorbing LiPSs, the peaks of S-Li (161.7 eV), S-S bond in Li_2S_6 (163.8 eV)[34] and sulfate (168.8 eV)[35] emerged, indicating LiPS was adsorbed by L-AG and partially oxidized to sulfate. Besides, N-Li bond (403.5 eV (Figure S10))[20] and O-Li bond (532.7 eV (Figure S11))[36] also imply the strong adsorption ability of both -NH_2 and -COOH with LiPSs.

The swelling ability of binder, which is essential for Li-ion diffusion and electrochemical reaction kinetics of the fabricated electrode,[37-38] was tested and shown in Figure S12. The sulfur-based cathodes were fabricated using sulfur powder (56 wt%) as the active material, BP2000 (24 wt%) and graphene (10 wt%) as the conductive additive, and different binders (10 wt%). The simultaneous use of BP2000 and graphene is intended to build a point-to-plane contact conductive network, which is more effective than individual spherical or layered carbon materials.[39] The electrode with L-AG shows an electrolyte uptake of around 250 wt%, which is much higher than that with AG and close to the swelling ability of PVDF. It's inferred that the introduced -NH_2 and -COOH help form a cross-linked binder network and incorporate more electrolyte into the chain of L-AG, resulting in larger electrolyte uptake[37] and thus better ion diffusion kinetics.[40] Moreover, the viscosities (Figure S13) of the 10 wt% solutions of all three binders are below 40 cp without obvious differences.

The adherence force test was further performed to display the electrode stability with different binders. An 8 × 8 grid (area size 1 mm × 1 mm) was drawn by a cross-cutting knife and the electrode materials were quickly peeled off from the Al foil by 3M tape (Figure 2a). As shown in Figure 2b-d, the cathode materials with PVDF have been peeled off around the scratches after drawing, while the electrodes using AG and L-AG still present the black color of cathode materials. As shown in Figure 2e-g, after peeling by 3 M tape, the active materials were peeled off in electrodes with PVDF so the silver color of Al foil is observed, while the electrodes with AG and L-AG still show the black color of cathode materials. It seems that the particular 3D grafted backbone of AG improves adherence force of cathode materials with current collector.[23] Compared with AG (21.6%), the even lower weight loss of L-AG electrodes (14.8%) suggests that mechanical strength is further reinforced by the assistance of the hydrogen bonding force between the oxygen-containing groups (-OH and -COOH) (Figure 2h).

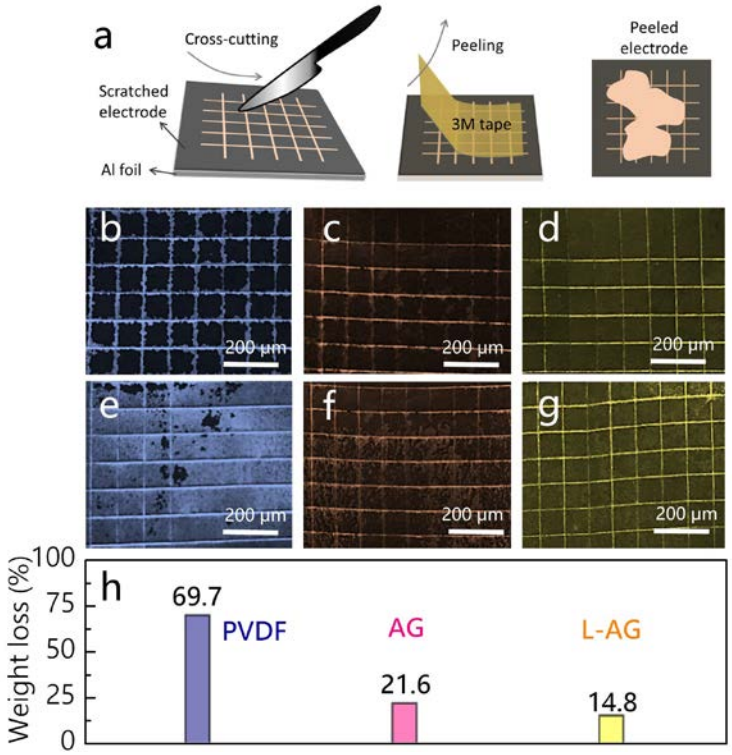

Figure 2. (a) A schematic illustration of the adherence force test. Images of electrodes before adherence force test using (b) PVDF, (c) AG and (d) L-AG binders, and images of electrodes after peeling using (e) PVDF, (f) AG and (g) L-AG binders. (h) The weight losses of electrodes after adherence test.

The electrode morphologies with the above three different binders were further characterized by scanning electron microscopy (SEM). As shown in Figure 3a-c, the assembled electrode with L-AG binder is much denser and has a much flatter surface without obvious cracks, suggesting the tight contact of sulfur, binder and the conductive additives in the electrode, which lowers the electron transfer resistance and then, improves the sulfur utilization. Moreover, the dense structure also helps confine the dissolved polysulfides in the electrode, improving the sulfur utilization and cycling stability. The electrode (Figure 3d) with PVDF binder shows a serious active material aggregation and generates many cracks after cycling, which should be attributed to the rigidity of PVDF that cannot buffer the volume changes of the electrode during the cycling.[41] In contrast, AG and L-AG binders are softer and more flexible to tolerate the volume changes of the sulfur-based electrode, as only a small number of cracks on the AG electrode and no crack on L-AG electrode surface is observed before and after cycling (Figure 3b, c, e, f). The magnified SEM images of the electrodes with PVDF, AG and L-AG binders after 100 cycles and the corresponding sulfur elemental mappings are shown in Figure S14. Sulfur is evenly distributed in the electrode with the L-AG binder (Figure S14f), indicating L-AG helps form a more stable 3D binder network and the active materials are uniformly distributed in the electrode. In all, L-AG shows superior adherence force and ability to stabilize the electrode structure.

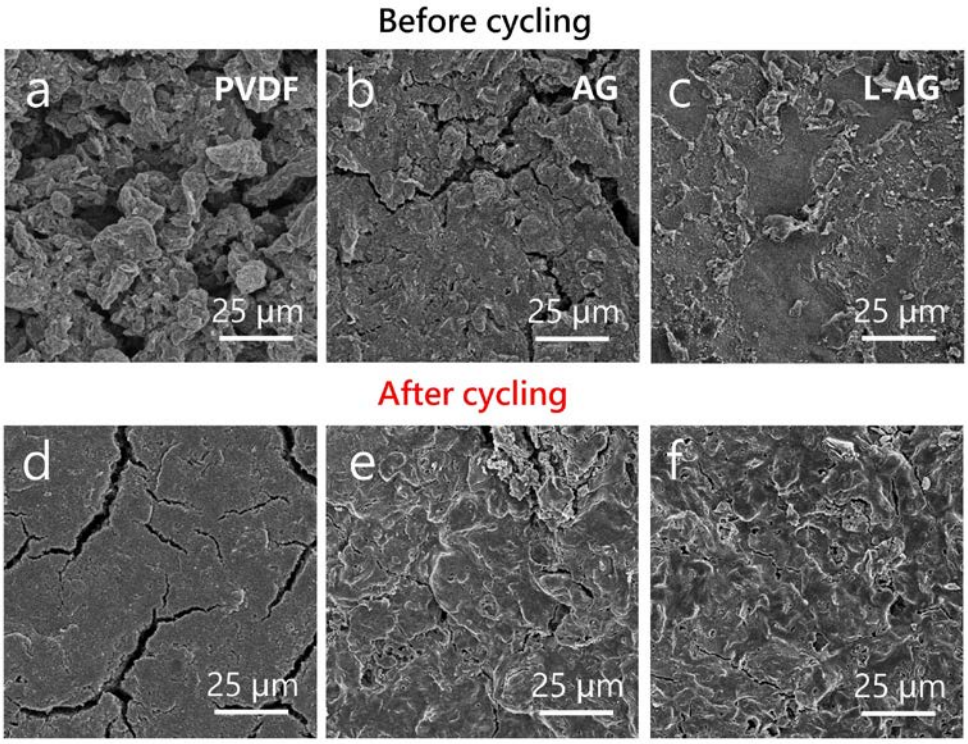

Figure 3. SEM images of the electrodes with PVDF, AG and L-AG binders before (a-c) and after the cycling (d-f).

The electrochemical stability of L-AG is confirmed by CV at 0.1 mV s^{-1} in the voltage range of 1.7-2.8 V. As shown in Figure S15, no reaction peaks appeared, which confirms the electrochemical stability of L-AG in the voltage window of Li-S batteries. To further evaluate the performance of Li-S batteries with different binders, the CV profiles of the batteries using AG and L-AG binders were measured (Figure S16a). There are two reduction peaks (2.3 V and 2.1 V) and one oxidation peak (2.4 V) in CV profiles, which are derived from the soluble long-chain LiPSs, insoluble short-chain Li_2S_2/Li_2S and the conversion from Li_2S_2/Li_2S to LiPSs.[10] Compared with the electrode with the AG binder, the peaks of the electrode with L-AG binder become stronger and sharper, suggesting the promoted redox reaction of LiPSs reinforced by L-AG, because the L-AG not only restrains the LiPSs shuttling but also helps them contact closer with the conductive

carbon. Besides, the reduction peak of the electrode with L-AG binder shifts to higher potential, implying the better kinetics and improved reversibility. The rate capability of batteries with different binders are shown in Figure 4a. The battery with L-AG binder can reach a high capacity of 780 mAh g^{-1} at 0.5 C and 500 mAh g^{-1} at 2 C, which are higher than those of the batteries with PVDF or AG binder, further confirming the faster kinetics enabled by L-AG. In Figure S16b-d, the discharge curves exhibit typical two plateaus, which are in agreement with the peaks in the CV profiles. The electrode with L-AG binder shows flat and stable plateaus with lower polarization than those with PVDF and AG binders. The capacity contributions of corresponding plateaus with the three binders are further analyzed in Figure S17 and Figure 4b, again showing the high sulfur utilization of the electrode with the L-AG binder due to its strong trapping ability to LiPSs.

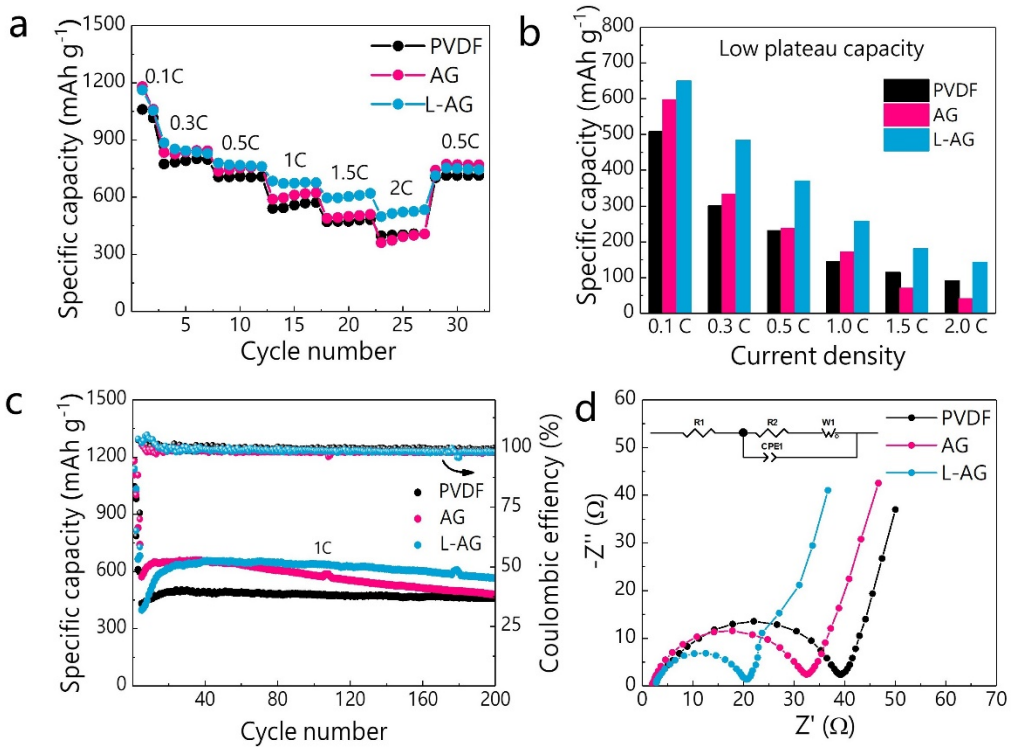

Figure 4. (a) The discharge capacities at various C rates (0.1 C to 2 C) using PVDF, AG and L-AG binders, and (b) shows the Low plateau capacities. (c) Cycling stability and Coulombic

efficiency of the electrodes with different binders at 1 C for 200 cycles. (d) Nyquist plots of them at the open circuit before cycling at room temperature.

Long-term cycling stability of the electrodes using the above three binders was tested at 1 C for 200 cycles (Figure 4c). The electrode with AG binder shows superior performance at the initial 60 cycles due to its grafted chain with oxygen-containing groups that lead to good adherence, while the discharge capacity subsequent declines can be attributed to the poor LiPSs anchoring ability. The electrode with L-AG binder delivers a discharge capacity of 654 mAh g^{-1} after the activation of the electrode. The capacity remains 564.7 mAh g^{-1} after 200 cycles with the Coulombic efficiency above 99% during cycling, corresponding to a capacity decay of 0.068% per cycle that much lower than that with PVDF and AG. The average CE of the battery with L-AG binder (98.7% at 1 C) is slightly lower than that with PVDF (99.5% at 1 C), which should be ascribed to the unavoidable side reactions between the oxygen groups in L-AG with Li ions.[42] In addition, the much higher sulfur utilization with the L-AG binder also leads to the slightly heavier dissolution of LiPSs in the electrolyte, and thus, the slightly lower CE. The increase of the capacity during the initial cycling should be mainly ascribed to the activation of the electrode, which was also shown in many other works.[43-44] A high sulfur loading (3 mg cm^{-2}) electrode with L-AG shows an initial capacity of 585 mAh g^{-1} and 507 mAh g^{-1} after 250 cycles at 1 C (Figure S18), with a small capacity decay of 0.053% per cycle. The stable cycling performance of L-AG battery can be ascribed to the superior LiPSs trapping ability of L-AG, which effectively suppresses the loss of active sulfur and facilitates the ion transport during the redox reaction. In addition, the smaller semicircle in the high frequency region of Nyquist plot (Figure 4d) suggests the decrease of the charge transfer resistance because of its better binding ability to maintain the integrity of the electrode structure. The fitted equivalent circuit is shown in the inset of Figure 4d. The R_1, R_2,

CPE_1 and W_1 represent the resistance of the electrolyte solution, the charge-transfer resistance, the related capacitance and the Li-ion diffusion Warburg impedance, respectively. The values of each part are listed in Table S1. The charge-transfer resistance of the electrode with L-AG (18.06 Ω) is much lower than those with PVDF (38.38 Ω) and AG (28.86 Ω), which should be the main reason leading to the much higher sulfur utilization and capacity of the battery with L-AG binder.

To investigate the effects of binders on the lithium ion diffusion in the electrode, CV measurements were conducted under different scan rates from 0.2 to 0.8 mV s^{-1} (Figure S19a-c).[45-46] The linear relationships between the currents of the Peak 1, Peak 2 and Peak 3 (I_p) with $v^{1/2}$ are shown in Figure S19d-f, suggesting the reaction in the cathodes with different binders is a diffusion-controlled process.[47-48] It can be seen the electrode with L-AG shows larger slop in Peak 1 and Peak 2 than those with AG and PVDF binders, demonstrating the lower ion diffusion resistance of the electrode with L-AG. But for Peak 3, the slope of the electrode with L-AG is smaller than that with AG, which was possibly ascribed to its stronger binding ability restraining the diffusion of LiPSs.

CONCLUSIONS

In summary, a water-soluble L-AG binder was prepared by simple and facile reaction between L-Cys and AG which introduced the $-NH_2$ and -COOH branches on the AG chains, largely enhancing the adsorption ability towards LiPSs and endowing the ability to build the cross-linked and flexible binder network in the electrode. The L-AG binder also improves cathode materials adhesion and shows large electrolyte uptake, contributing to the even distribution of active materials and fast Li ion diffusion, thus enhancing the reaction kinetics. Besides, as a grafted polymer, L-AG can build a highly flexible network to accommodate the volume change of sulfur during cycling and maintain the electrode integrity, preventing the electrode structure from

collapsing. As a result, the Li-S battery with L-AG binder shows improved rate performance and cyclic stability than those with PVDF and AG binders. Overall, this work presents a simple method to prepare a multifunctional binder and shows a promising strategy to promote the practical applications of Li-S batteries.

ASSOCIATED CONTENT

Supporting Information

The following files are available free of charge. The synthesis process of L-AG, SEM images, FTIR spectra, TG profiles, XPS profiles of L-AG, AG, and L-Cys, geometries of Li_2S_4, Li_2S_6, AG and L-AG, viscosity of binder solutions, electrolyte uptake ability, weight loss, CV profiles, electrochemical performance. (PDF)

AUTHOR INFORMATION

Corresponding Author

*E-mail: lv.wei@sz.tsinghua.edu.cn

*E-mail: gaomin@cat.hokudai.ac.jp

Author Contributions

‡Qi Qi, Yaqian Deng and Sichen Gu contributed equally to this work.

ACKNOWLEDGMENT

This work was supported by the National Natural Science Foundation of China (51772164), Cooperative Research Program of Institute for Catalysis, Hokkaido University (Grant 19B1024),

the Local Innovative and Research Teams Project of Guangdong Pearl River Talents Program (2017BT01N111), Guangdong Natural Science Funds for Distinguished Young Scholars (2017B030306006), the Guangdong Special Support Program (2017TQ04C664), Shenzhen Basic Research Project (No. JCYJ20170412171359175), the Shenzhen graphene manufacturing innovation center (201901161513) and the Photo-excitonix Project in Hokkaido University, the MEXT project "Integrated Research on Chemical Synthesis", "Priority Issue on Post-K Computer" (Development of new fundamental technologies for high-efficiency energy creation, conversion/storage anduse). A part of the computations was performed at RCCS (Okazaki, Japan) and ACCMS (Kyoto University).

REFERENCES

1. Ji, X.; Nazar, L. F., Advances in Li-S batteries. *J. Mater. Chem.* **2010,** *20* (44), 9821-9826.
2. Bruce, P. G.; Freunberger, S. A.; Hardwick, L. J.; Tarascon, J.-M., Li-O_2 and Li-S Batteries with High Energy Storage. *Nat. Mater.* **2011,** *11*, 19-29.
3. Chung, W. J.; Griebel, J. J.; Kim, E. T.; Yoon, H.; Simmonds, A. G.; Ji, H. J.; Dirlam, P. T.; Glass, R. S.; Wie, J. J.; Nguyen, N. A.; Guralnick, B. W.; Park, J.; Somogyi, Á.; Theato, P.; Mackay, M. E.; Sung, Y.-E.; Char, K.; Pyun, J., The Use of Elemental Sulfur as an Alternative Feedstock for Polymeric Materials. *Nat. Chem.* **2013,** *5*, 518-524.
4. Manthiram, A.; Fu, Y.; Su, Y.-S., Challenges and Prospects of Lithium-Sulfur Batteries. *Acc. Chem. Res.* **2013,** *46* (5), 1125-1134.
5. Liang, Y.; Zhao, C.-Z.; Yuan, H.; Chen, Y.; Zhang, W.; Huang, J.-Q.; Yu, D.; Liu, Y.; Titirici, M. M.; Chueh, Y.-L.; Yu, H.; Zhang, Q., A Review of Rechargeable Batteries for Portable Electronic Devices. *InfoMat* **2019,** *1* (1), 6-32.
6. Fan, X.; Liu, X.; Hu, W.; Zhong, C.; Lu, J., Advances in the Development of Power Supplies for the Internet of Everything. *InfoMat* **2019,** *1* (2), 130-139.
7. Vizintin, A.; Chabanne, L.; Tchernychova, E.; Arcon, I.; Stievano, L.; Aquilanti, G.; Antonietti, M.; Fellinger, T.-P.; Dominko, R., The Mechanism of Li_2S Activation in Lithium-Sulfur Batteries: Can We Avoid the Polysulfide Formation? *J. Power Sources* **2017,** *344*, 208-217.
8. Li, G.; Wang, S.; Zhang, Y.; Li, M.; Chen, Z.; Lu, J., Revisiting the Role of Polysulfides in Lithium-Sulfur Batteries. *Adv. Mater.* **2018,** *30* (22), 1705590
9. Shi, H.; Lv, W.; Zhang, C.; Wang, D.-W.; Ling, G.; He, Y.; Kang, F.; Yang, Q.-H., Functional Carbons Remedy the Shuttling of Polysulfides in Lithium-Sulfur Batteries: Confining, Trapping, Blocking, and Breaking Up. *Adv. Funct. Mater.* **2018,** *28* (38), 1800508.
10. Zhou, T.; Lv, W.; Li, J.; Zhou, G.; Zhao, Y.; Fan, S.; Liu, B.; Li, B.; Kang, F.; Yang, Q.-H., Twinborn TiO_2-TiN Heterostructures Enabling Smooth Trapping-Diffusion-Conversion of

Polysulfides Towards Ultralong Life Lithium-Sulfur Batteries. *Energy Environ. Sci.* **2017,** *10* (7), 1694-1703.
11. Gueon, D.; Hwang, J. T.; Yang, S. B.; Cho, E.; Sohn, K.; Yang, D.-K.; Moon, J. H., Spherical Macroporous Carbon Nanotube Particles with Ultrahigh Sulfur Loading for Lithium-Sulfur Battery Cathodes. *ACS Nano* **2018,** *12* (1), 226-233.
12. Zhao, Q.; Zhu, Q.; Miao, J.; Guan, Z.; Liu, H.; Chen, R.; An, Y.; Wu, F.; Xu, B., Three-Dimensional Carbon Current Collector Promises Small Sulfur Molecule Cathode with High Areal Loading for Lithium-Sulfur Batteries. *ACS Appl. Mater. Inter.* **2018,** *10* (13), 10882-10889.
13. Zhang, J.; Shi, Y.; Ding, Y.; Peng, L.; Zhang, W.; Yu, G., A Conductive Molecular Framework Derived Li_2S/N, P-Codoped Carbon Cathode for Advanced Lithium-Sulfur Batteries. *Adv. Energy Mater.* **2017,** *7* (14), 1602876.
14. Wang, N.; Xu, Z.; Xu, X.; Liao, T.; Tang, B.; Bai, Z.; Dou, S., Synergistically Enhanced Interfacial Interaction to Polysulfide via N, O Dual-Doped Highly Porous Carbon Microrods for Advanced Lithium-Sulfur Batteries. *ACS Appl. Mater. Inter.* **2018,** *10* (16), 13573-13580.
15. Vizintin, A.; Guterman, R.; Schmidt, J.; Antonietti, M.; Dominko, R., Linear and Cross-Linked Ionic Liquid Polymers as Binders in Lithium-Sulfur Batteries. *Chem. Mater.* **2018,** *30* (15), 5444-5450.
16. Bao, W.; Zhang, Z.; Gan, Y.; Wang, X.; Lia, J., Enhanced Cyclability of Sulfur Cathodes in Lithium-Sulfur Batteries with Na-alginate as a Binder. *J. Energy Chem.* **2013,** *22* (5), 790-794.
17. He, M.; Yuan, L.-X.; Zhang, W.-X.; Hu, X.-L.; Huang, Y.-H., Enhanced Cyclability for Sulfur Cathode Achieved by a Water-Soluble Binder. *J. Phys. Chem. C* **2011,** *115* (31), 15703-15709.
18. Lacey, M. J.; Jeschull, F.; Edstrom, K.; Brandell, D., Why PEO as a Binder or Polymer Coating Increases Capacity in the Li-S System. *Chem. Commun.* **2013,** *49* (76), 8531-8533.
19. Fu, X.; Scudiero, L.; Zhong, W.-H., A Robust and Ion-Conductive Protein-Based Binder Enabling Strong Polysulfide Anchoring for Highenergy Lithium-Sulfur Batteries. *J. Mater. Chem. A* **2019,** *7* (4), 1835-1848.
20. Chen, W.; Lei, T.; Qian, T.; Lv, W.; He, W.; Wu, C.; Liu, X.; Liu, J.; Chen, B.; Yan, C.; Xiong, J., A New Hydrophilic Binder Enabling Strongly Anchoring Polysulfides for High-Performance Sulfur Electrodes in Lithium-Sulfur Battery. *Adv. Energy Mater.* **2018,** *8* (12), 1702889.
21. Yan, L.; Gao, X.; Thomas, J. P.; Ngai, J.; Altounian, H.; Leung, K. T.; Meng, Y.; Li, Y., Ionically cross-linked PEDOT: PSS as a Multifunctional Conductive Binder for High-Performance Lithium-Sulfur Batteries. *Sustain. Energ. Fuels* **2018,** *2* (7), 1574-1581.
22. Randall, R.; Phillips, G.; Williams, P., Fractionation and Characterization of Gum from Acacia Senegal. *Food Hydrocolloid.* **1989,** *3* (1), 65-75.
23. Li, G.; Ling, M.; Ye, Y.; Li, Z.; Guo, J.; Yao, Y.; Zhu, J.; Lin, Z.; Zhang, S., Acacia Senegal-Inspired Bifunctional Binder for Longevity of Lithium-Sulfur Batteries. *Adv. Energy Mater.* **2015,** *5* (21), 1500878.
24. Seh, Z. W.; Zhang, Q.; Li, W.; Zheng, G.; Yao, H.; Cui, Y., Stable Cycling of Lithium Sulfide Cathodes Through Strong Affinity with A Bifunctional Binder. *Chem. Sci.* **2013,** *4* (9), 3673-3677.
25. Frisch, M. J.; Trucks, G. W.; Schlegel, H. B.; Scuseria, G. E.; Robb, M. A.; Cheeseman, J. R.; Scalmani, G.; Barone, V.; Mennucci, B.; Petersson, G. A., Gaussian 09, Rev. C. 01; Gaussian. *Inc.: Wallingford, CT* **2010**.

26. Reed, A. E.; Weinhold, F., Natural Bond Orbital Analysis of Near-Hartree-Fock Water Dimer. *J. Chem. Phys.* **1983,** *78* (6), 4066-4073.
27. Reed, A. E.; Weinstock, R. B.; Weinhold, F., Natural Population Analysis. *J. Chem. Phys.* **1985,** *83* (2), 735-746.
28. Wang, W.; Rusin, O.; Xu, X.; Kim, K. K.; Escobedo, J. O.; Fakayode, S. O.; Fletcher, K. A.; Lowry, M.; Schowalter, C. M.; Lawrence, C. M., Detection of Homocysteine and Cysteine. *J. Am. Chem. Soc.* **2005,** *127* (45), 15949-15958.
29. Rodante, F.; Marrosu, G., Thermal Analysis of Some α-amino Acids Using Simultaneous TG-DSC Apparatus. The Use of Dynamic Thermogravimetry to Study the Chemical Kinetics of Solid State Decomposition. *Thermochim. Acta* **1990,** *171*, 15-29.
30. Ling, M.; Zhang, L.; Zheng, T.; Feng, J.; Guo, J.; Mai, L.; Liu, G., Nucleophilic Substitution Between Polysulfides and Binders Unexpectedly Stabilizing Lithium Sulfur Battery. *Nano Energy* **2017,** *38*, 82-90.
31. Rocklin, R. D.; Pohl, C. A., Determination of Carbohydrates by Anion Exchange Chromatography with Pulsed Amperometric Detection. *J. Liq. Chromatogr.* **1983,** *6* (9), 1577-1590.
32. Ling, M.; Yan, W.; Kawase, A.; Zhao, H.; Fu, Y.; Battaglia, V. S.; Liu, G., Electrostatic Polysulfides Confinement to Inhibit Redox Shuttle Process in the Lithium Sulfur Batteries. *ACS Appl. Mater. Inter.* **2017,** *9* (37), 31741-31745.
33. Alassaf, S.; Phillips, G. O., Hydrocolloids: structure-function relationships. *Food Sci. Tech-Brazil* **2009,** *23* (3), 17-20.
34. Liao, J.; Ye, Z., Quaternary Ammonium Cationic Polymer as a Superior Bifunctional Binder for Lithium-Sulfur Batteries and Effects of Counter Anion. *Electrochim. Acta* **2018,** *259*, 626-636.
35. Liang, X.; Hart, C.; Pang, Q.; Garsuch, A.; Weiss, T.; Nazar, L. F., A Highly Efficient Polysulfide Mediator for Lithium-Sulfur Batteries. *Nat. Commun.* **2015,** *6*, 5682.
36. Du, P.; Lu, J.; Lau, K. C.; Luo, X.; Bareno, J.; Zhang, X.; Ren, Y.; Zhang, Z.; Curtiss, L. A.; Sun, Y.-K.; Amine, K., Compatibility of Lithium Salts with Solvent of the Non-Aqueous Electrolyte in Li-O_2 Batteries. *Phys. Chem. Chem. Phys.* **2013,** *15* (15), 5572-5581.
37. Yan, L.; Gao, X.; Wahid-Pedro, F.; Quinn, J. T. E.; Meng, Y.; Li, Y., A Novel Epoxy Resin-Based Cathode Binder for Low Cost, Long Cycling Life, and High-Energy Lithium-Sulfur Batteries. *J. Mater. Chem. A* **2018,** *6* (29), 14315-14323.
38. Zhou, G.; Liu, K.; Fan, Y.; Yuan, M.; Liu, B.; Liu, W.; Shi, F.; Liu, Y.; Chen, W.; Lopez, J.; Zhuo, D.; Zhao, J.; Tsao, Y.; Huang, X.; Zhang, Q.; Cui, Y., An Aqueous Inorganic Polymer Binder for High Performance Lithium-Sulfur Batteries with Flame-Retardant Properties. *ACS Central Sci.* **2018,** *4* (2), 260-267.
39. Wang, H.; Yang, Y.; Liang, Y.; Robinson, J. T.; Li, Y.; Jackson, A.; Cui, Y.; Dai, H., Graphene-Wrapped Sulfur Particles as a Rechargeable Lithium–Sulfur Battery Cathode Material with High Capacity and Cycling Stability. *Nano Lett.* **2011,** *11* (7), 2644-2647.
40. Akhtar, N.; Shao, H.; Ai, F.; Guan, Y.; Peng, Q.; Zhang, H.; Wang, W.; Wang, A.; Jiang, B.; Huang, Y., Gelatin-Polyethylenimine Composite as a Functional Binder for Highly Stable Lithium-Sulfur Batteries. *Electrochim. Acta* **2018,** *282*, 758-766.
41. Dirlam, P. T.; Glass, R. S.; Char, K.; Pyun, J., The Use of Polymers in Li-S Batteries: A Review. *J. Polym. Sci. Pol. Chem.* **2017,** *55* (10), 1635-1668.
42. de Godoi, F. C.; Wang, D.-W.; Zeng, Q.; Wu, K.-H.; Gentle, I. R., Dependence of $LiNO_3$ Decomposition on Cathode Binders in Li-S Batteries. *J. Power Sources* **2015,** *288*, 13-19.

43. Xu, G.; Yan, Q.-b.; Kushima, A.; Zhang, X.; Pan, J.; Li, J., Conductive Graphene Oxide-Polyacrylic Acid (GOPAA) Binder for Lithium-Sulfur Battery. *Nano Energy* **2017,** *31*, 568-574.
44. Wang, D.; Wang, K.; Wu, H.; Luo, Y.; Sun, L.; Zhao, Y.; Wang, J.; Jia, L.; Jiang, K.; Li, Q.; Fan, S.; Wang, J., CO_2 Oxidation of Carbon Nanotubes for Lithium-Sulfur Batteries With Improved Electrochemical Performance. *Carbon* **2018,** *132*, 370-379.
45. Xia, Y.; Mathis, T. S.; Zhao, M.-Q.; Anasori, B.; Dang, A.; Zhou, Z.; Cho, H.; Gogotsi, Y.; Yang, S., Thickness-Independent Capacitance of Vertically Lligned Liquid-Crystalline MXenes. *Nature* **2018,** *557* (7705), 409-412.
46. Chen, W.; Lei, T.; Lv, W.; Hu, Y.; Yan, Y.; Jiao, Y.; He, W.; Li, Z.; Yan, C.; Xiong, J., Atomic Interlamellar Ion Path in High Sulfur Content Lithium-Montmorillonite Host Enables High-Rate and Stable Lithium-Sulfur Battery. *Adv. Mater.* **2018,** *30* (40), 1804084.
47. Hu, Y.; Chen, W.; Lei, T.; Zhou, B.; Jiao, Y.; Yan, Y.; Du, X.; Huang, J.; Wu, C.; Wang, X.; Wang, Y.; Chen, B.; Xu, J.; Wang, C.; Xiong, J., Carbon Quantum Dots-Modified Interfacial Interactions and Ion Conductivity for Enhanced High Current Density Performance in Lithium-Sulfur Batteries. *Adv. Energy Mater.* **2019,** *9* (7), 1802955.
48. Lei, T.; Chen, W.; Lv, W.; Huang, J.; Zhu, J.; Chu, J.; Yan, C.; Wu, C.; Yan, Y.; He, W.; Xiong, J.; Li, Y.; Yan, C.; Goodenough, J. B.; Duan, X., Inhibiting Polysulfide Shuttling with a Graphene Composite Separator for Highly Robust Lithium-Sulfur Batteries. *Joule* **2018,** *2* (10), 2091-104.

TOC

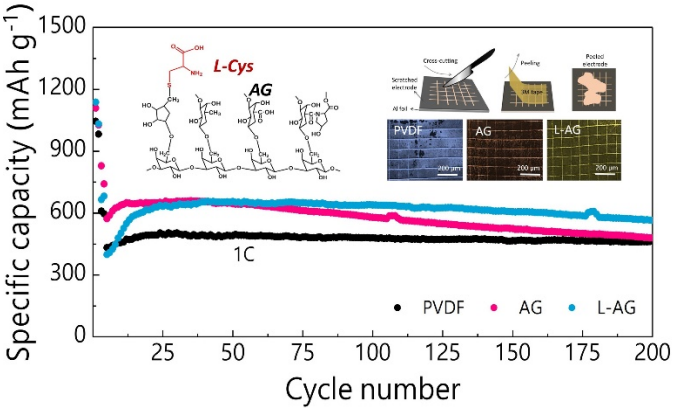
Specific capacity (mAh g-1)
1500
1200
900
600
300
0
25
50
75
100
125
150
175
200
Cycle number
L-Cys
AG
1C
PVDF
AG
L-AG
Cross-cutting
Peeling
Pocket electrode
Scratched electrode
Al foil
3M tape
PVDF
AG
L-AG
200 μm
200 μm
200 μm